Supporting Information

Active Site Tuning Based on Pseudo-Binary Alloys for Low-Temperature Acetylene Semihydrogenation

Jiamin Ma,[a,†] Feilong Xing,[a] Ken-ichi Shimizu,[a] and Shinya Furukawa[a,†,*]

a Institute for Catalysis, Hokkaido University, N-21, W-10, Sapporo 001-0021, Japan
† present address: Division of Applied Chemistry, Graduate School of Engineering, Osaka University, Osaka 565-0871, Japan

E-mail: furukawa@chem.eng.osaka-u.ac.jp,

Tel: +81-6-6879-7808

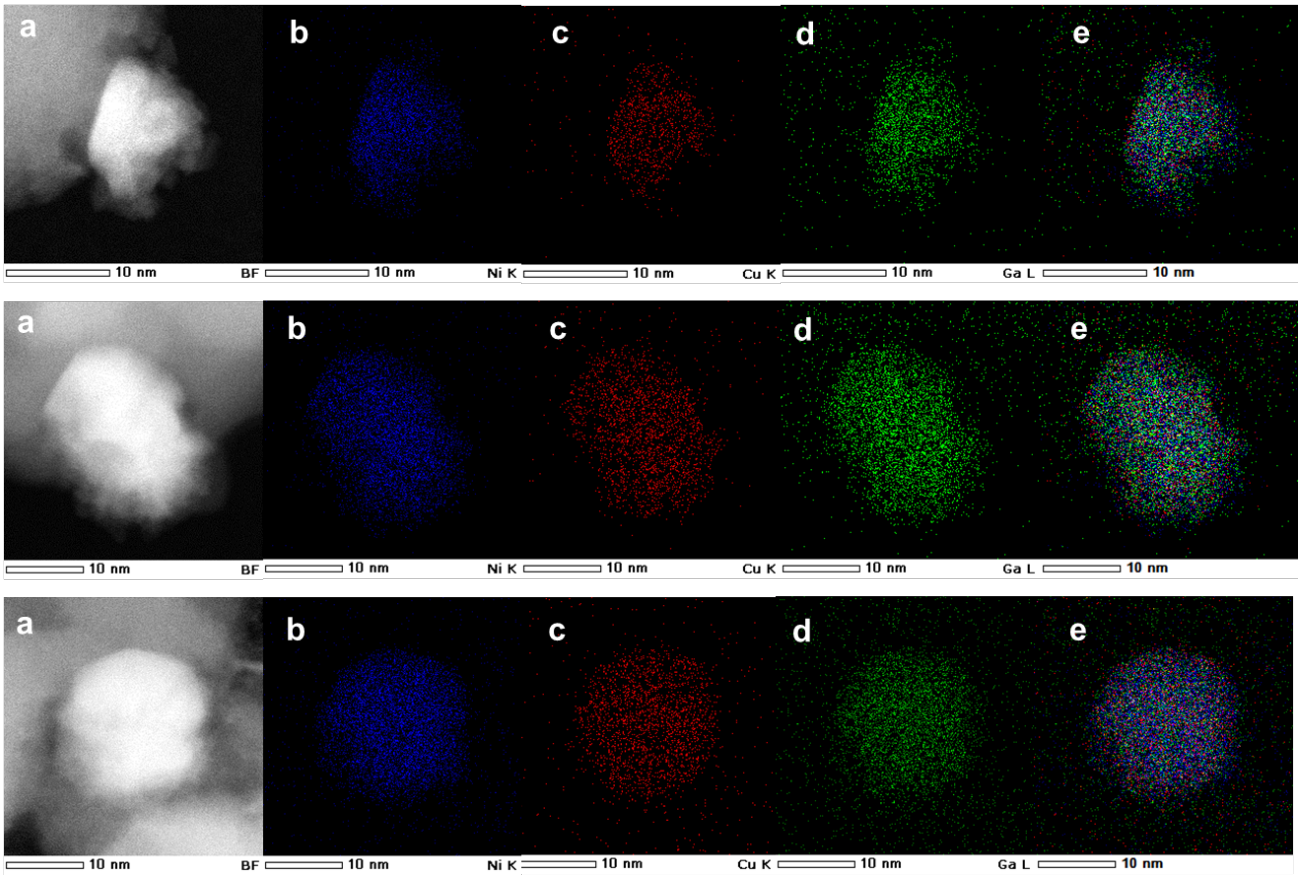

Figure S1. (a) HAADF–STEM image and the corresponding elemental maps for (b) Ni, (c) Cu, (d) Ga, (e) Ni+Cu+Ga (magnified for a few particles) for $(Ni_{0.8}Cu_{0.2})_3Ga/TiO_2$.

Table S1. Particle size of $(Ni_{0.8}Cu_{0.2})_3Ga/TiO_2$, $(Ni_{0.8}Cu_{0.2})_3Ga/SiO_2$ and Ni_3Ga/TiO_2 calculated according to Scherrer equation.

catalysts	Scherrer constant	half with / degree	center / degree	crystallite size / nm
$(Ni_{0.8}Cu_{0.2})_3Ga/TiO_2$		0.76	43.52	10.6
Ni_3Ga/TiO_2	0.849	1.03	43.74	7.8
$(Ni_{0.8}Cu_{0.2})_3Ga/SiO_2$		1.60	43.74	5.1

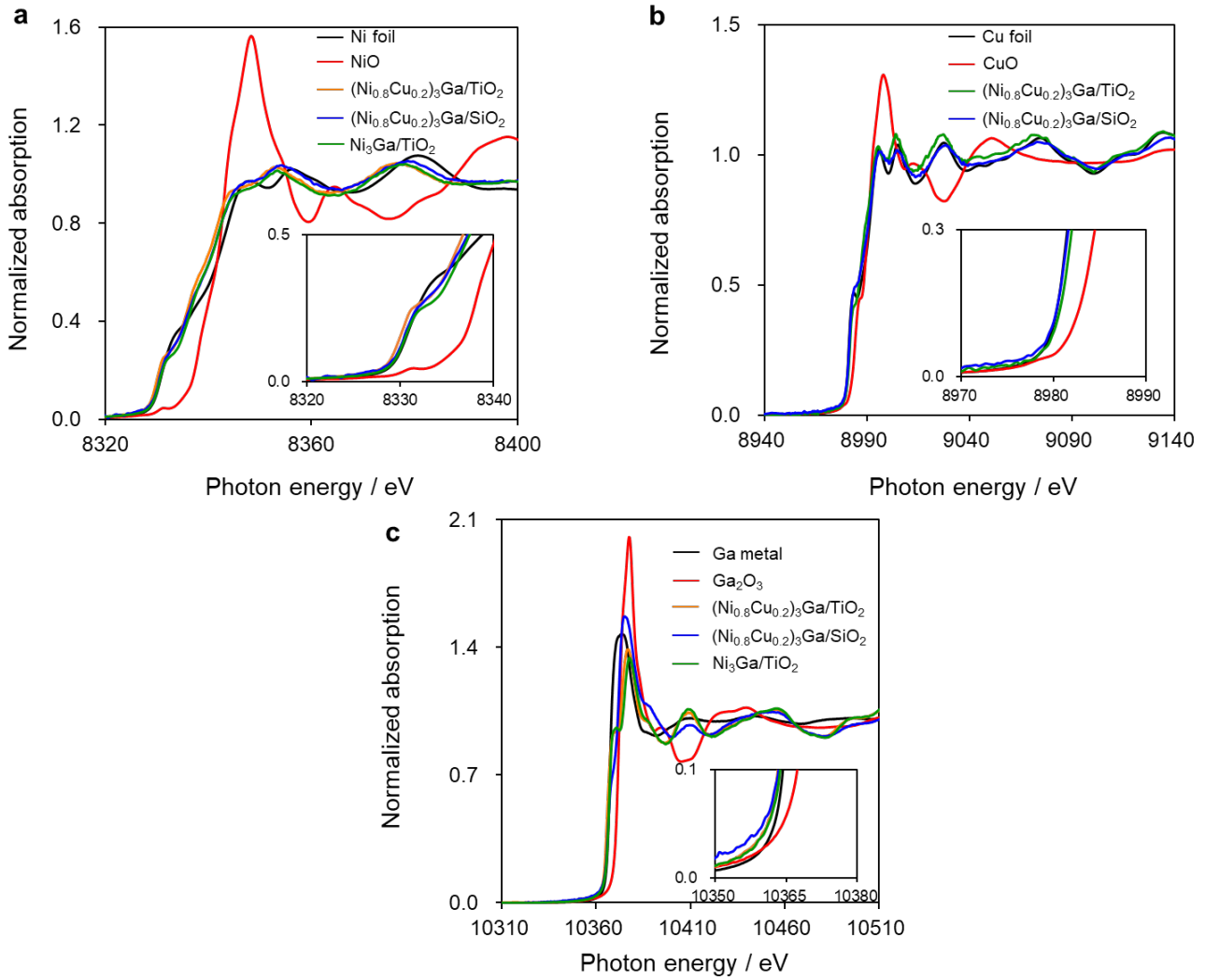

Figure S2. (a) Ni, (b) Cu, and (c) Ga K-edge XANES spectra of over $(Ni_{0.8}Cu_{0.2})_3Ga/TiO_2$, $(Ni_{0.8}Cu_{0.2})_3Ga/SiO_2$, Ni_3Ga/TiO_2 and reference compounds.

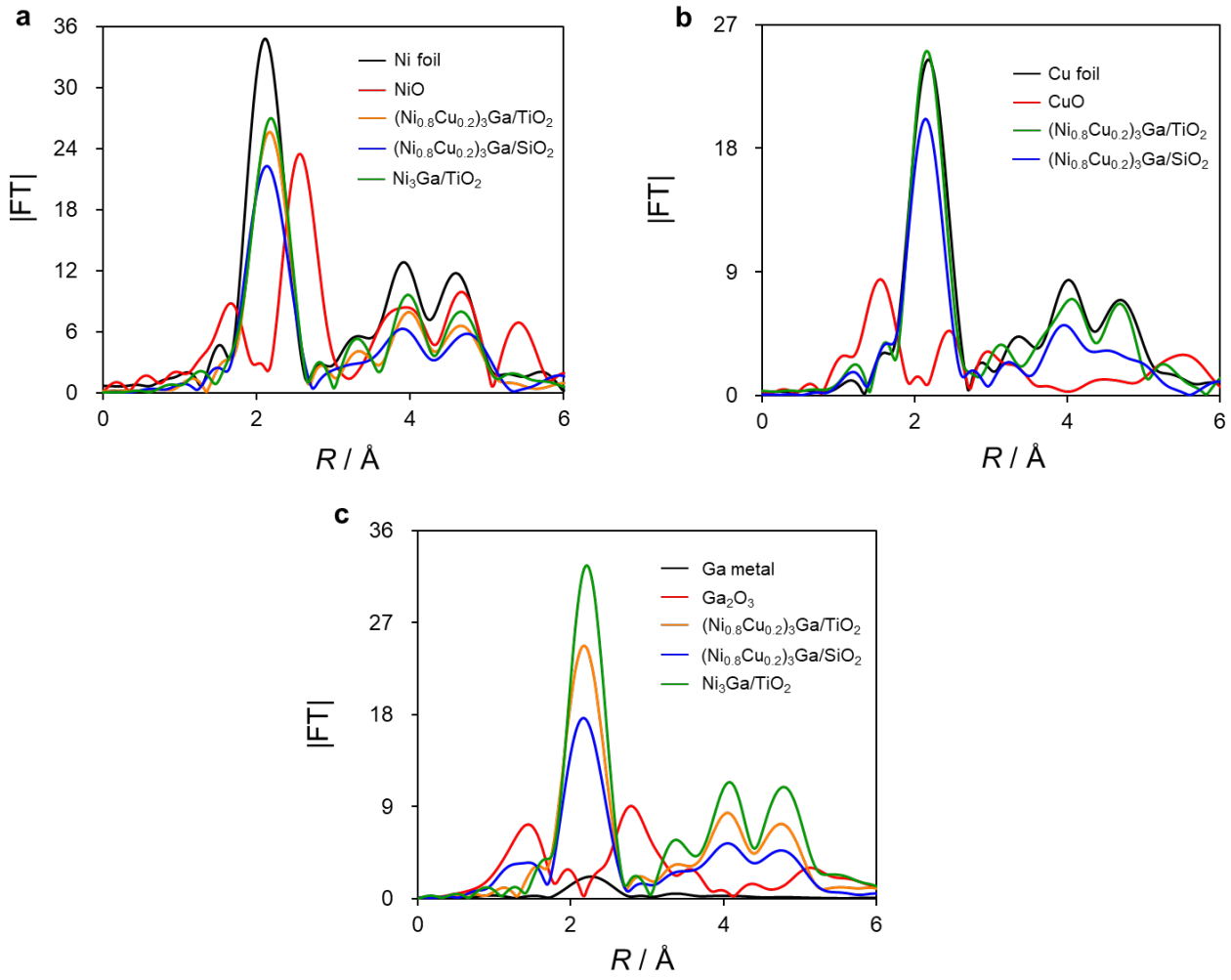

Figure S3. Fourier-transforms of EXAFS in (a) Ni, (b) Cu, and (c) Ga K-edge over $(Ni_{0.8}Cu_{0.2})_3Ga/TiO_2$, $(Ni_{0.8}Cu_{0.2})_3Ga/SiO_2$, Ni_3Ga/TiO_2. and reference compounds.

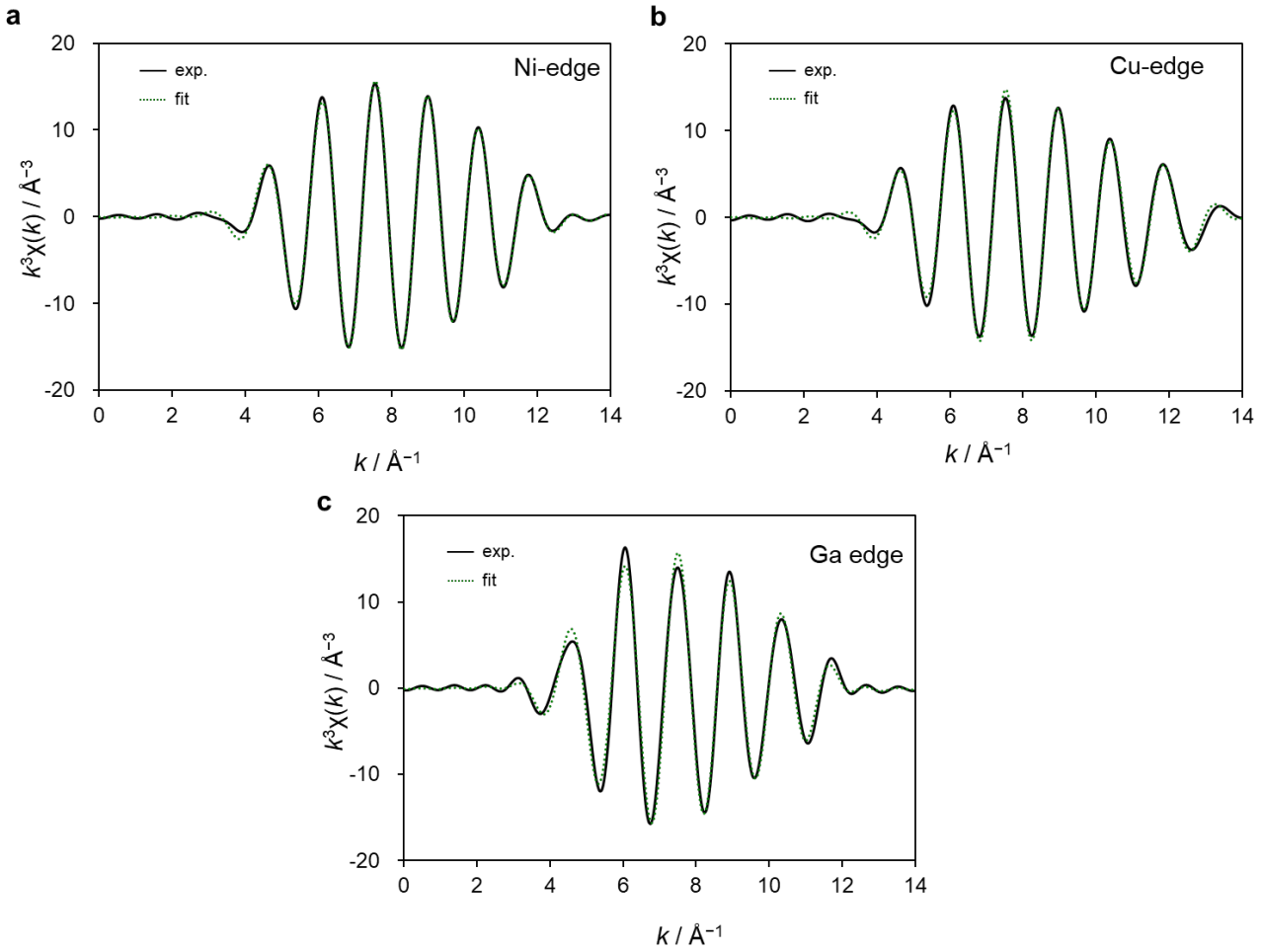

Figure S4. Curve-fitting results of (a) Ni (b) Cu and (c) Ga K-edge k^3-weighted EXAFS of $(Ni_{0.8}Cu_{0.2})_3Ga/TiO_2$. Solid and dashed lines indicate the results of simulation and experiment, respectively.

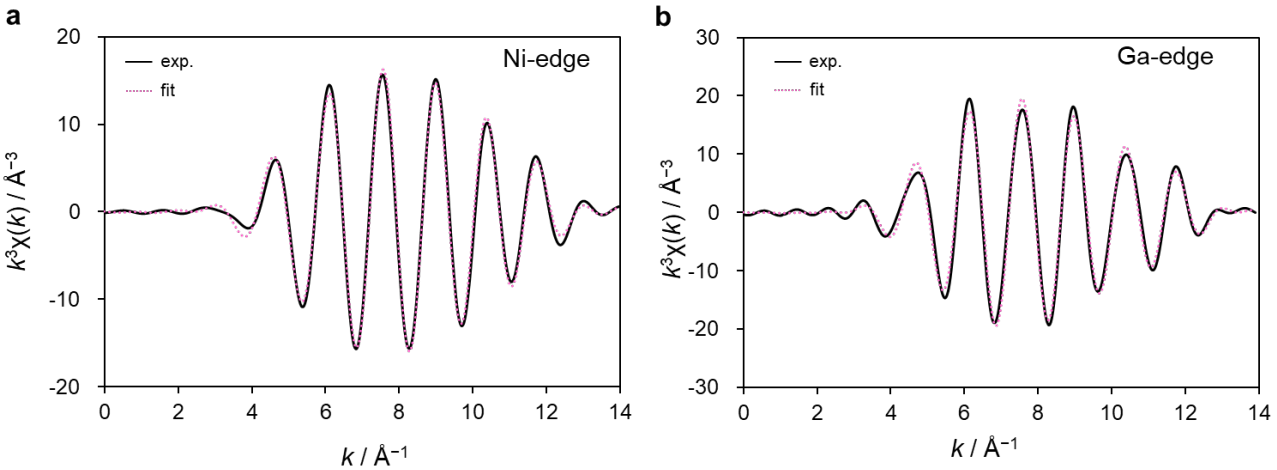

Figure S5. Curve-fitting results of (a) Ni and (b) Ga K-edge k^3-weighted EXAFS of Ni_3Ga/TiO_2. Solid and dashed lines indicate the results of simulation and experiment, respectively.

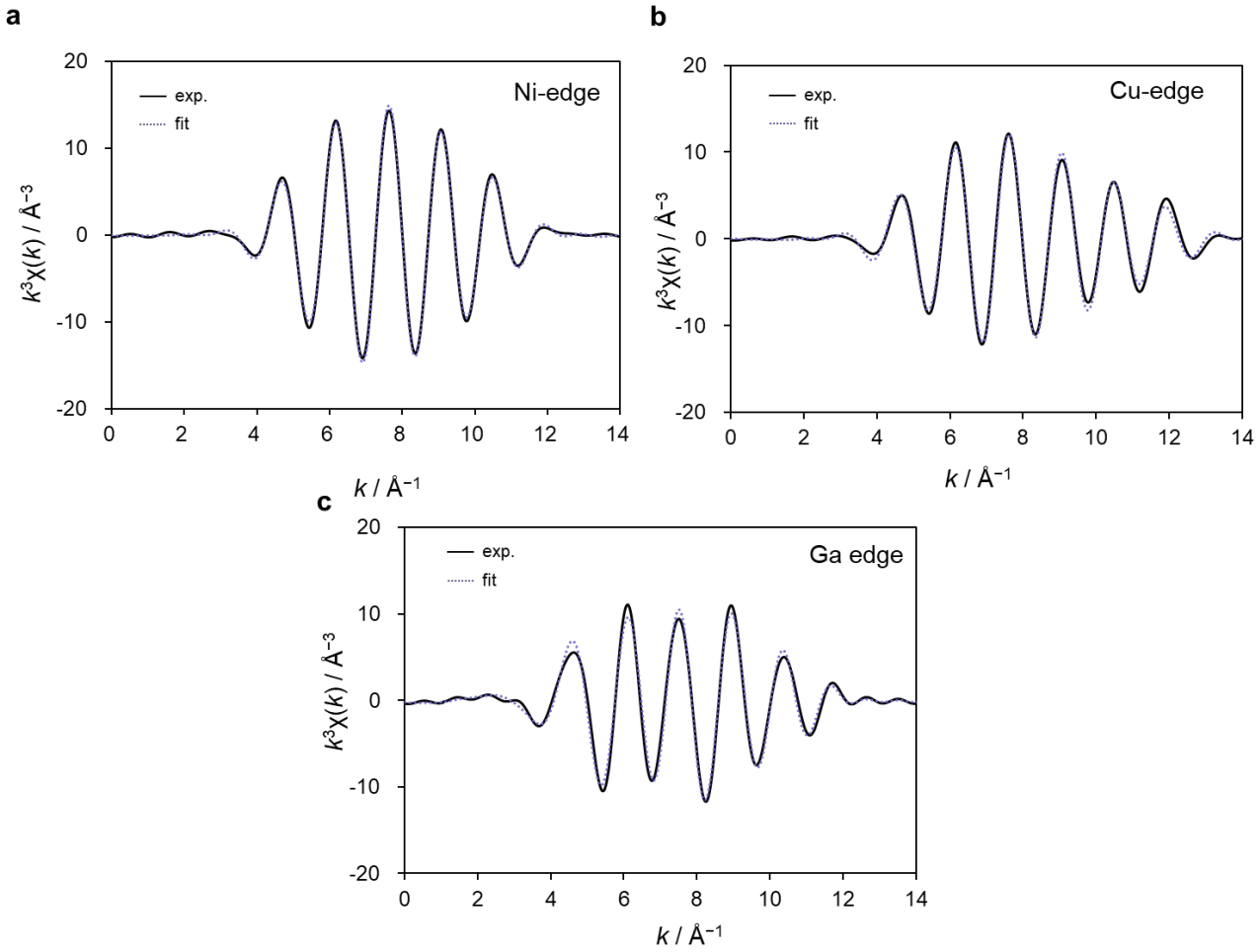

Figure S6. Curve-fitting results of (a) Ni (b) Cu and (c) Ga K-edge k^3-weighted EXAFS of $(Ni_{0.8}Cu_{0.2})_3Ga/SiO_2$. Solid and dashed lines indicate the results of simulation and experiment, respectively.

Table S2. Summary of the EXAFS curve fitting for $(Ni_{0.8}Cu_{0.2})_3Ga/TiO_2$, $(Ni_{0.8}Cu_{0.2})_3Ga/SiO_2$, Ni_3Ga/TiO_2 catalysts and reference.

Sample	Edge	Shell	S_o^2	CN	r (Å)	ΔE_o (eV)	σ^2 (Å^2)	R-factor
Ni foil	Ni k	Ni-Ni	0.846	12	2.48±0.01	5.43±0.7	0.00621	0.003
Cu foil	Cu k	Cu-Cu	0.918	12	2.54±0.02	6.26±0.9	0.0088	0.005
Ga_2O_3	Ga k	Ga-O	1.316	3	1.91±0.09	6.84±1.8	0.00657	0.014
		Ga-O		1	2.12±0.25		0.00361	
		Ga-Ga		2	3.05±0.01		0.00338	
$(Ni_{0.8}Cu_{0.2})_3Ga/TiO_2$	Ni k	Ni-Ga	0.846	3.50±0.99	2.46±0.07	5.40±1.5	0.00415	0.003
		Ni-Ni(Cu)		7.00±0.99	2.58±0.08		0.00472	
	Cu k	Cu-Ga	0.918	2.79±0.48	2.49±0.04	2.81±1.8	0.00275	0.008
		Cu-Cu(Ni)		8.38±0.48	2.60±0.04		0.00799	
	Ga k	Ga-O	1.316	2.11±0.29	2.03±0.20	0.65±1.7	0.0698	0.005
		Ga-Ni(Cu)		8.46±0.28	2.54±0.00		0.00914	
$(Ni_{0.8}Cu_{0.2})_3Ga/SiO_2$	Ni k	Ni-Ga	0.846	3.29±0.64	2.43±0.11	4.51±1.1	0.00185	0.018
		Ni-Ni(Cu)		6.58±0.64	2.57±0.04		0.00323	
	Cu k	Cu-Ga	0.918	3.59±0.93	2.29±0.24	9.38±2.3	0.02631	0.01
		Cu-Cu(Ni)		10.8±0.93	2.50±0.05		0.00953	
	Ga k	Ga-O	1.316	1.47±0.20	1.81±0.01	1.91±1.6	0.00796	0.02
		Ga-Ni(Cu)		5.89±0.20	2.54±0.00		0.00897	
Ni_3Ga/TiO_2	Ni k	Ni-Ga	0.846	3.51±1.22	2.45±0.09	6.27±1.9	0.00421	0.006
		Ni-Ni		7.03±1.23	2.57±0.04		0.00389	
	Ga k	Ga-O	1.316	2.28±1.10	1.79±0.04	5.20±1.5	0.13945	0.021
		Ga-Ni		9.11±1.12	2.53±0.00		0.00811	

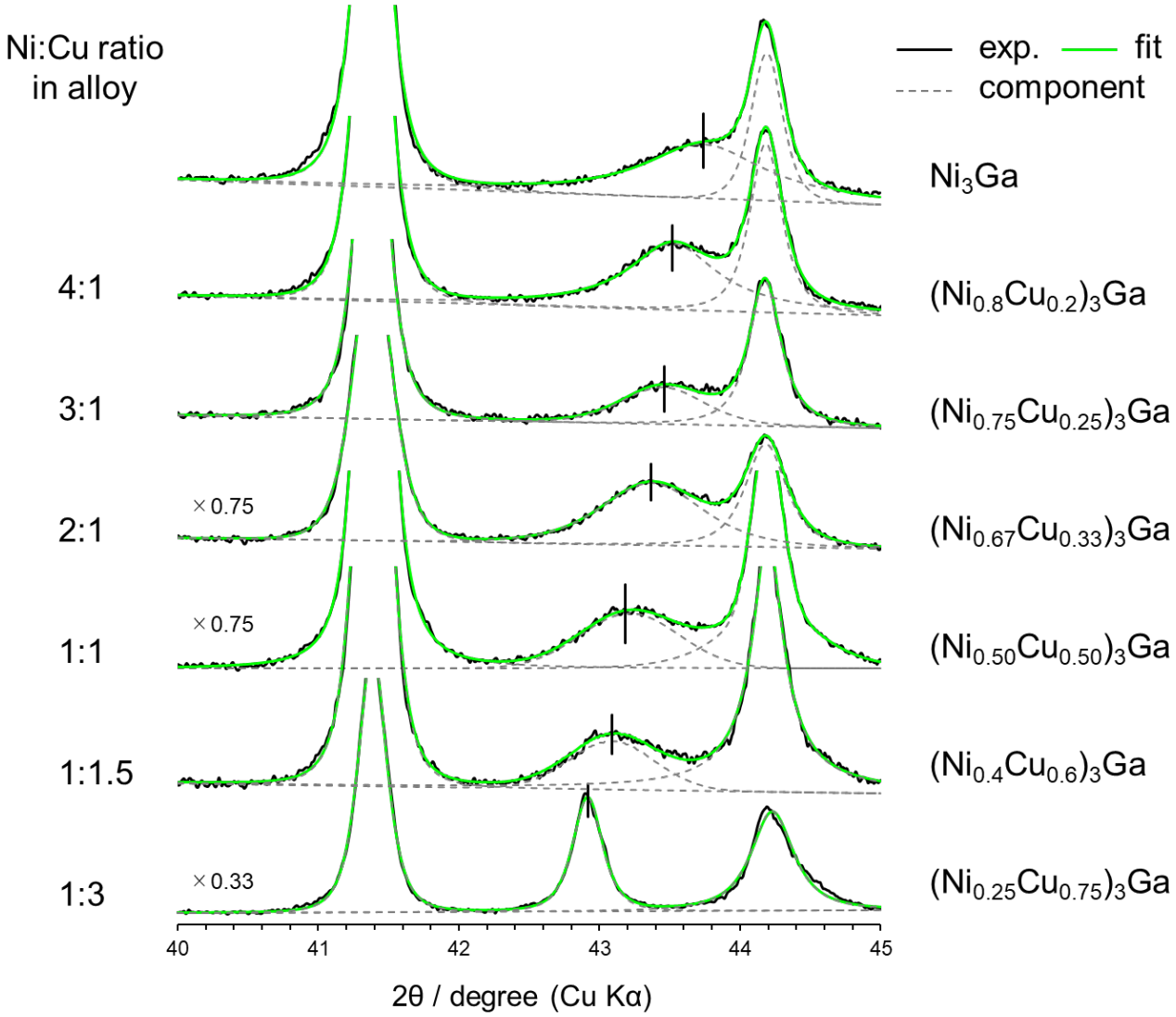

Figure S7. XRD analysis for $(Ni_{1-x}Cu_x)_3Ga/TiO_2$ (x = 0, 0.2, 0.25, 0.33, 0.5, 0.6, 0.75) catalysts. Vertical solid lines indicate the diffraction angles of the corresponding $(Ni_{1-x}Cu_x)_3Ga$ phases.

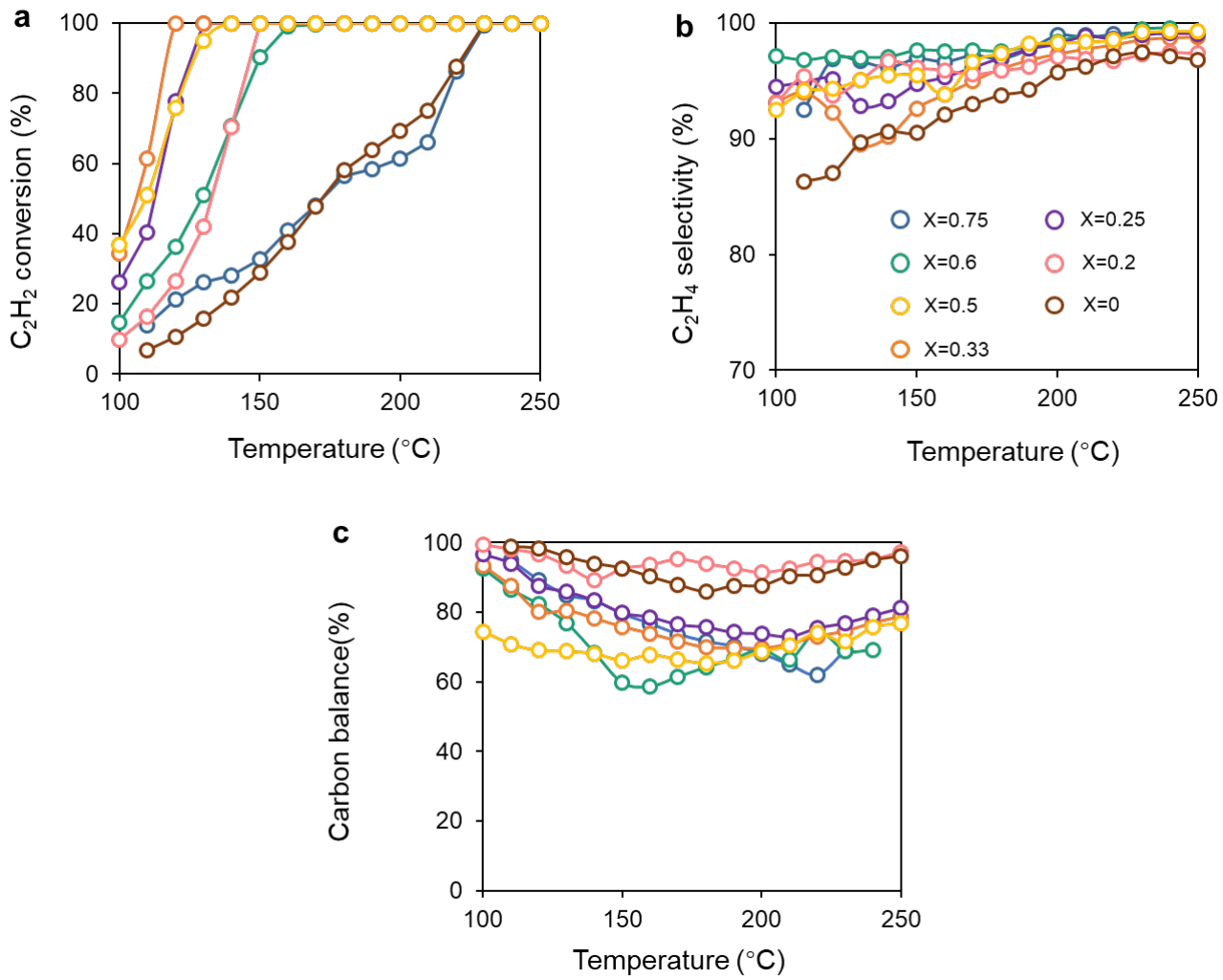

Figure S8. (a) C_2H_2 conversion, (b) C_2H_4 selectivity and (c) carbon balance as a function of reaction temperature over $(Ni_{1-x}Cu_x)_3Ga/TiO_2$.

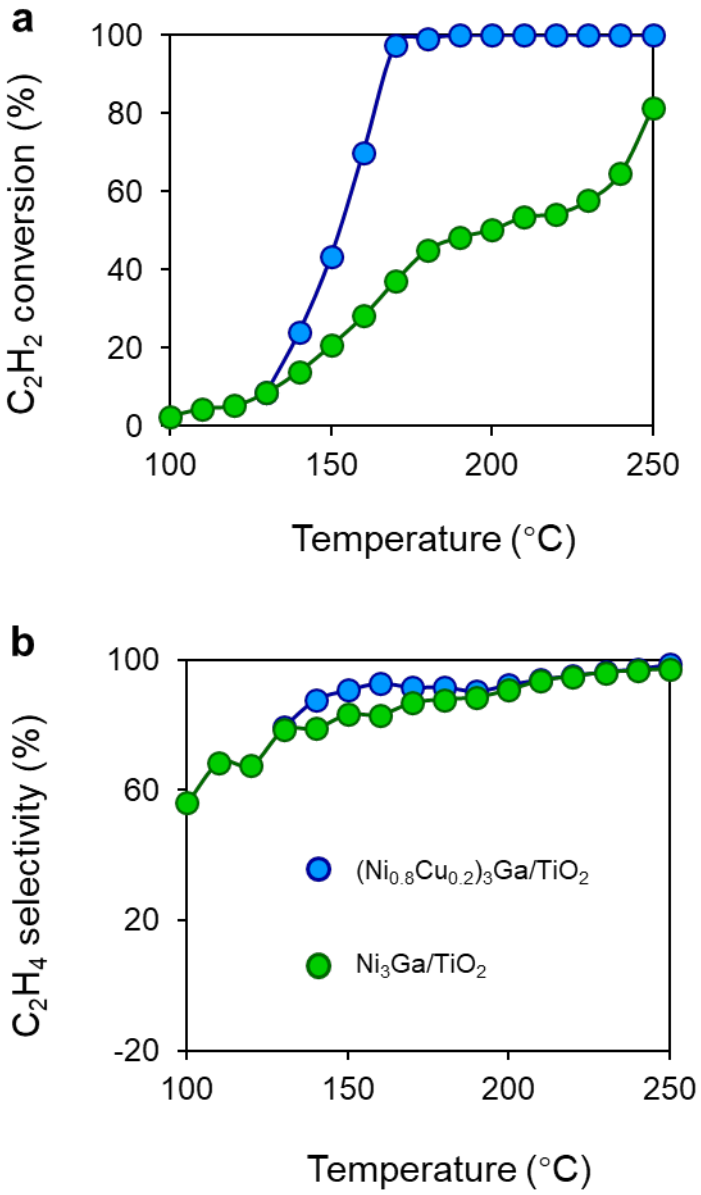

Figure S9. (a) C_2H_2 conversion and (b) C_2H_4 selectivity as a function of reaction temperature in the presence of ethylene (C_2H_2:H_2:He:C_2H_4 = 1:10:39:5 $mLmin^{-1}$) over $(Ni_{0.8}Cu_{0.2})_3Ga/TiO_2$ and Ni_3Ga/TiO_2.

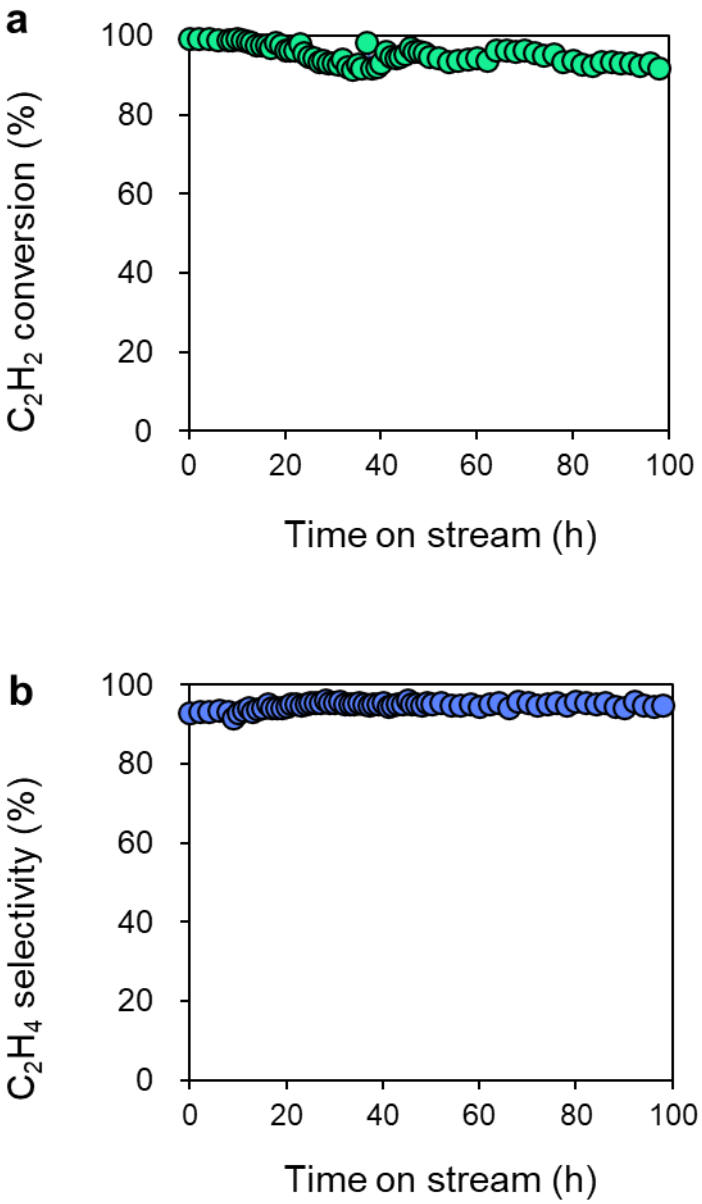

Figure S10. Long-term stability test using $(Ni_{0.8}Cu_{0.2})_3Ga/TiO_2$ in the presence of excess ethylene (C_2H_2:H_2:He:C_2H_4 = 1:10:39:5 $mLmin^{-1}$) at 180°C. (a) C_2H_2 conversion and (b) C_2H_4 selectivity.

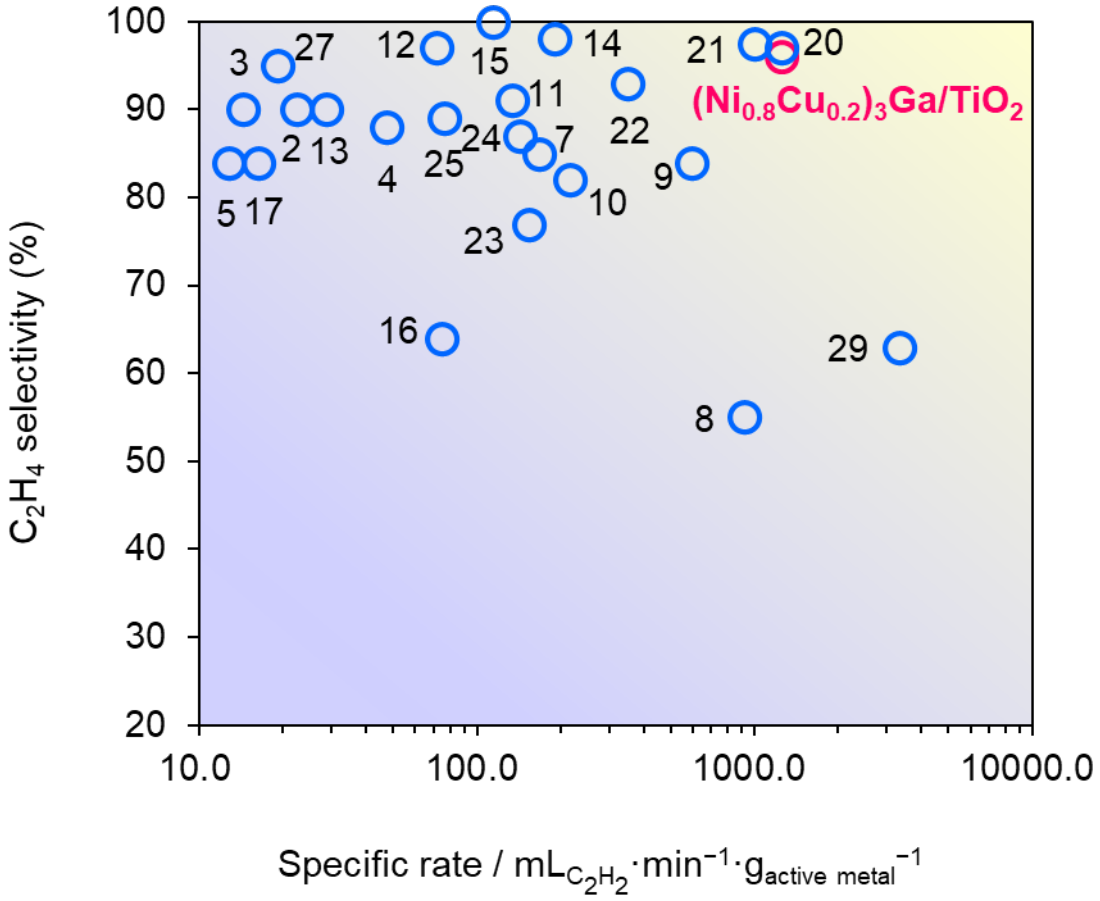

Figure S11. Relationship between the specific activity and ethylene selectivity at high acetylene conversion (>80%) for 3d transition metal-based catalysts that were reported in literature and developed in this study. Numbers correspond to the entries in Table S3.

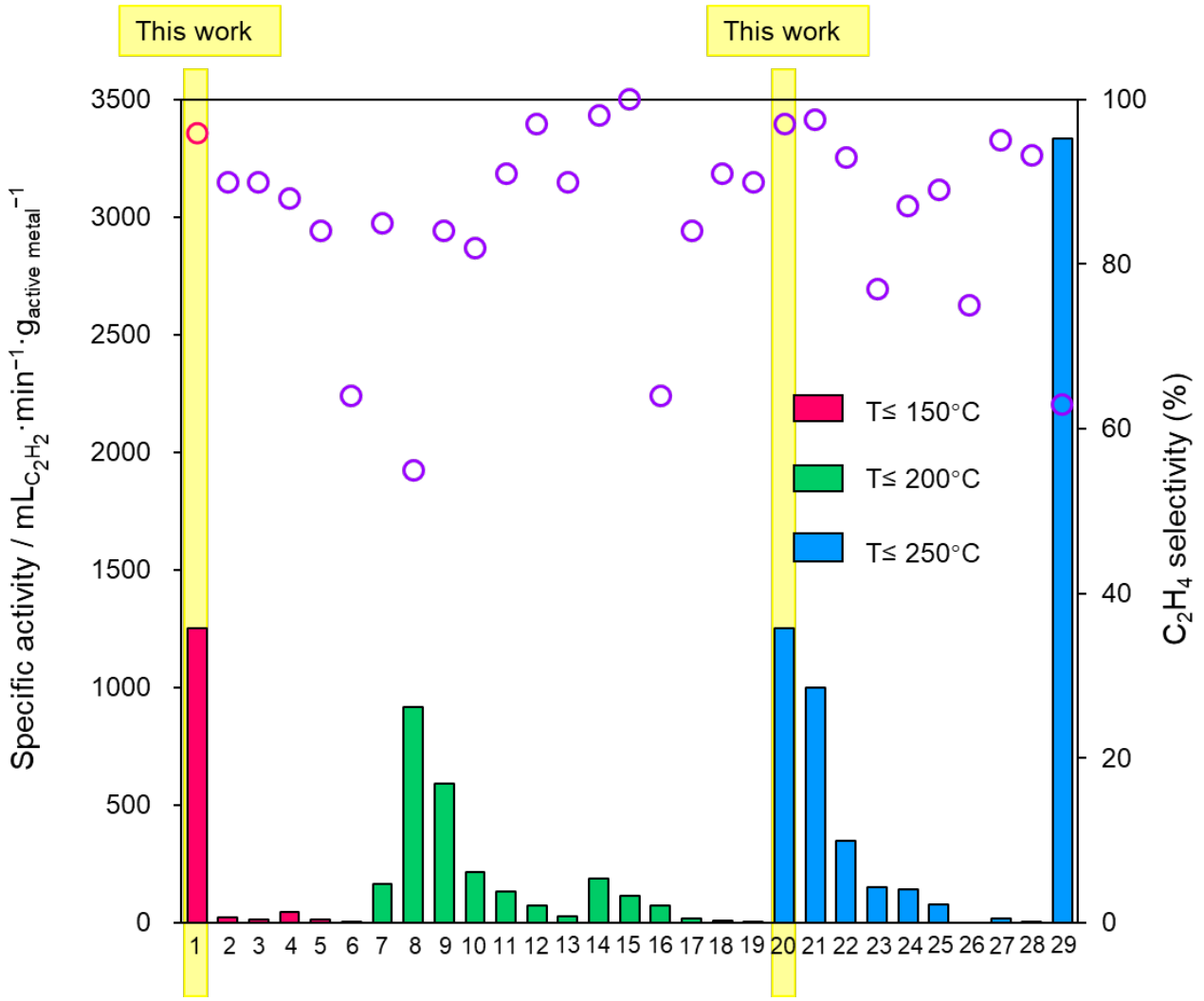

Figure S12. Relationship between the specific activity and ethylene selectivity at high acetylene conversion (>80%) at different reaction temperature for 3d transition metal-based catalysts that were reported in literature and developed in this study. Numbers correspond to the entries in Table S3.

Table S3. Summary of reaction conditions and catalytic performances in acetylene semihydrogenation using 3d transition metal-based catalysts that were reported in literature and developed in this study.

entry	catalyst	loading (wt%)	amount / mg	C_2H_2 flow /mLmin^{-1}	C_2H_2 : H_2 : C_2H_4	total flow /mLmin^{-1}	GHSV / mLg^{-1}h^{-1}	conv. (%)	sel. (%)	temp. / °C	specific rate / mL$_{C2H2}$min^{-1}g$_M^{-1}$	Operation time (h)	ref
1	$(Ni_{0.8}Cu_{0.2})_3Ga/TiO_2$	1	80	1	1 : 10 : 0	50	37500	100	96	150	1250.0	60	This work
2	$Ni_3GaC_{0.5}$/MgAl LDH	14.88	150	0.5	0.5:2.5:10	100	40000	100	90	110	22.4	36	[1]
3	Ni_1MoS/Al_2O_3	3.5	500	0.2475	1:20:0	165	19800	100	90	125	14.1	16	[2]
4	NiCu/MgAl-MMO	9.58	100	0.558	1 : 2 : 103	166	100500	81	88	140	47.2	36	[3]
5	$Cu(OH)_2$	78.9	100	1	1 : 9 : 0	10	6000	100	84	110	12.7	250	[4]
6	Cu_2O	88.8	100	0.045	1 : 22 : 197	10	6000	100	64	120	0.5	100	[5]
7	$Ni_3ZnC_{0.7}/C$	12	50	1	1:15:0	100	120000	100	85	165	166.7	10	[6]
8	$AgNi_{0.5}/SiO_2$	1.09	30	0.3	1:20:0	30	60000	100	55	180	917.4	24	[7]
9	Ni/g-C_3N_4-T	1	50	0.3	1:10:20	30	36000	99	84	175	594.0	20	[8]
10	NiGa/MgAl-LDH	10	50	1.2	1 : 10 : 20	120	144000	90	82	190	216.0	24	[9]
11	$0.5Cu/Al_2O_3$	0.5	300	0.2	1 : 10 : 50	20	4000	100	91	188	133.3	40	[10]
12	Na-Ni/CHA	3.5	200	0.5	1 : 16 : 0	50	15000	100	97	170	71.4	20	[11]
13	$Ni_1Cu_2/g-C_3N_4$	3.5	150	0.15	1 : 10 : 50	30	12000	100	90	160	28.6	400	[12]
14	Cu_1/ND	0.25	200	0.1	1 : 10 : 20	10	3000	95	98	200	190.0	60	[13]
15	Ni–CeO_2	1.54	200	0.35	1 : 70 : 4	70	21000	100	100	200	113.6	3	[14]
16	Ni_6In/SiO_2	8	500	3	1 : 10 : 0	300	36000	100	64	200	75.0	35	[15]
17	$Al_{13}Fe_4$	38.9	20	0.15	1 : 10 : 100	30	90000	85	84	200	16.4	14	[16]
18	Ni-SAs/N-C	5.67	400	0.2	1 : 20 : 100	40	6000	96	91	200	8.5	18	[17]
19	Co_2FeGe	47.8	400	0.03	1 : 400 : 100	30	4500	91	90	200	0.1		[18]
20	Ni_3Ga/TiO_2	1	80	1	2 : 10 : 0	50	37500	100	97	230	1250.0	1	This work
21	NiCuFeGaGe/SiO_2	1	100	1	1 : 10 : 0	50	30000	100	98	220	1000.0	28	[19]
22	NiCu/ZrO_2	4.6	25	0.4	1:10:20	40	96000	100	93	220	347.8	15	[20]
23	$Ni_3Ga/MgAl_2O_4$	2	100	0.33	1 : 20 : 100	67	144000	92	77	220	153.3	24	[21]
24	Ni/MCM-41	25	100	3.7	1 : 2 : 0	66.6	40000	96	87	240	142.2	10	[22]
25	Ni_3Ge/MCM-41	3.2	1500	3.9	1 : 2.1 : 0	29	1160	94	89	250	76.4		[23]
26	$Cu_{2.75}Ni_{0.25}Fe$	-	150	0.63	1.5:4.5:8.1	42	16800	100	75	250		30	[24]
27	$Cu/Fe_{0.16}MgO_x$	18.0	200	0.69	1 :100 : 3	209	62700	100	95	215	19.2	40	[25]
28	NiSb/MgAl LDH	8.58	300	0.15	0.5:2.5:30	30	6000	100	93.2	260	5.8	48	[26]
29	$NiCu_{0.125}$/MCM-41	1	100	3.3	1 : 3 : 0	13.3	8000	100	63	250	3333.3	9	[27]

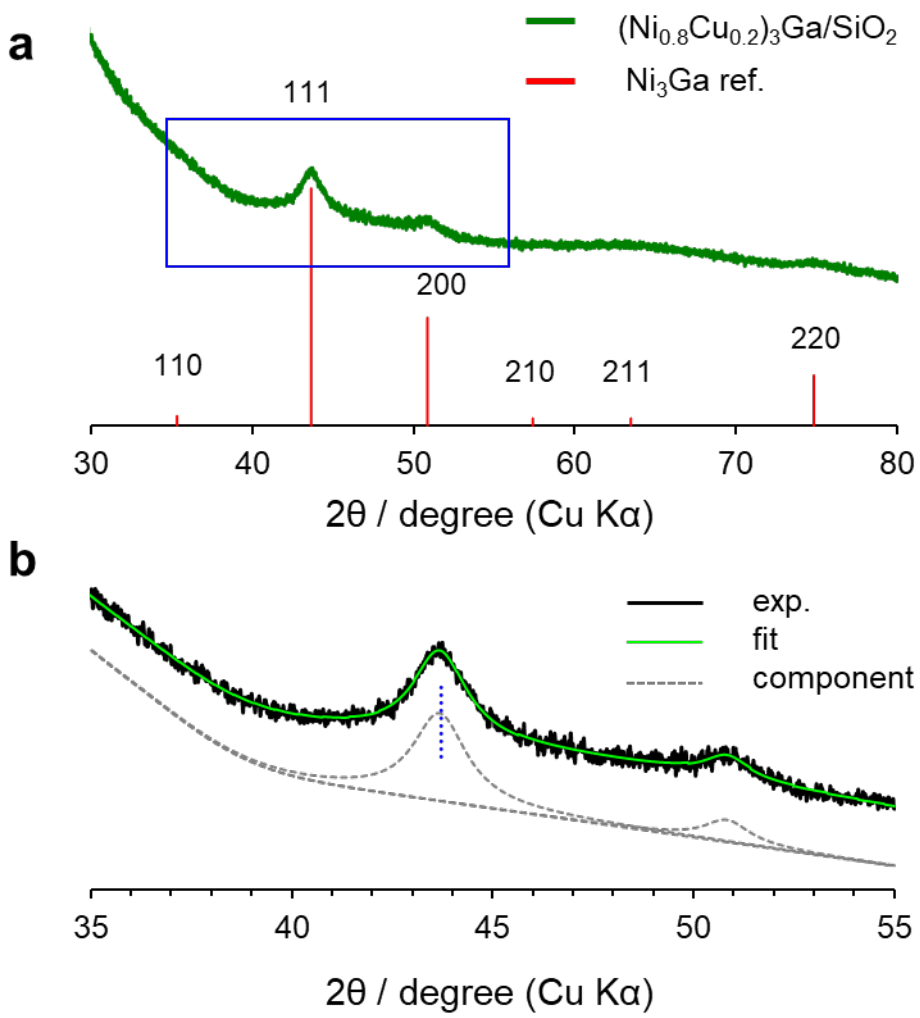

Figure S13. (a) XRD pattern of $(Ni_{0.8}Cu_{0.2})_3Ga/SiO_2$ and (b) its magnification indicated as the bule square. The center of 111 diffraction was at 43.72° (blue dotted line), which agreed with that of $(Ni_{0.8}Cu_{0.2})_3Ga/TiO_2$ (43.74°).

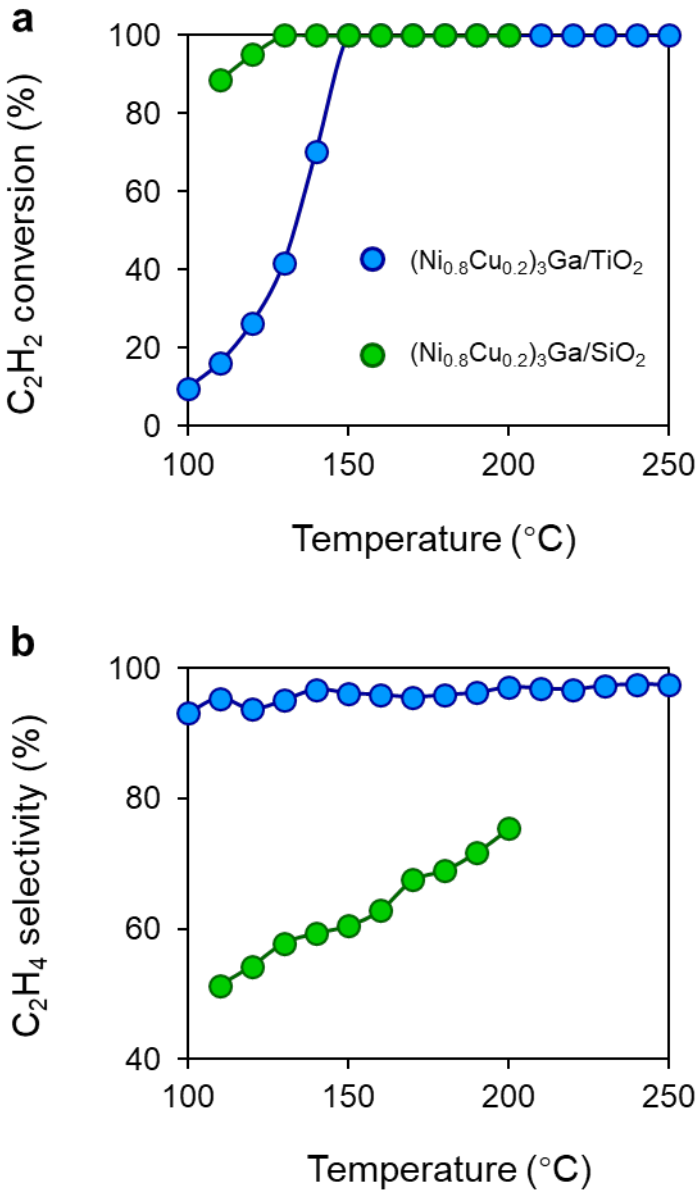

Figure S14. (a) C_2H_2 conversion and (b) C_2H_4 selectivity as a function of reaction temperature in the absence of ethylene (C_2H_2:H_2:He = 1:10:39 mLmin^{-1}) over $(Ni_{0.8}Cu_{0.2})_3Ga/TiO_2$ and $(Ni_{0.8}Cu_{0.2})_3Ga/SiO_2$.

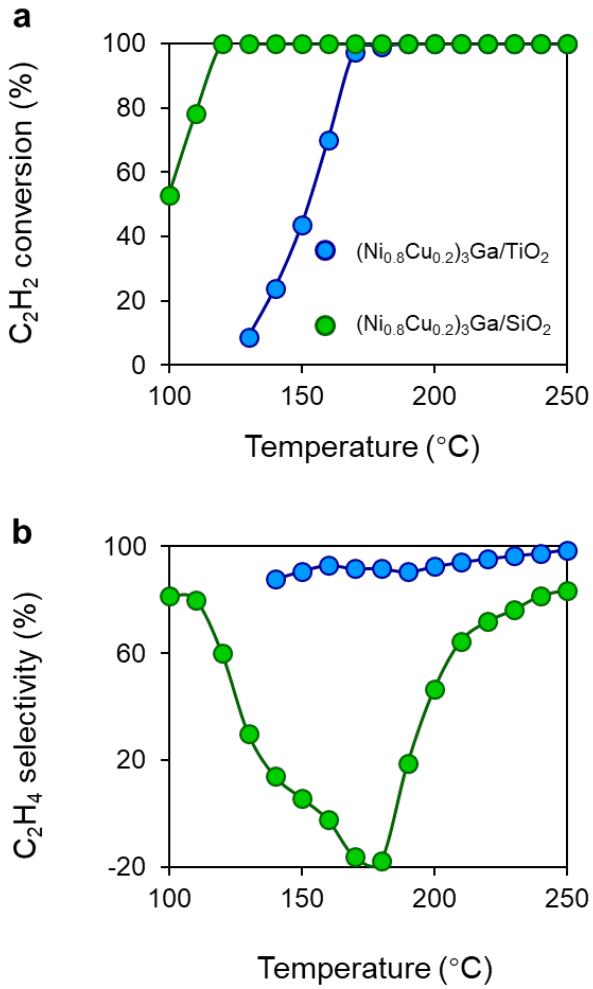

Figure S15. (a) C_2H_2 conversion and (b) C_2H_4 selectivity as a function of reaction temperature in the presence of ethylene (C_2H_2:H_2:He:C_2H_4 = 1:10:39:5 mLmin^{-1}) over $(Ni_{0.8}Cu_{0.2})_3Ga/TiO_2$ and $(Ni_{0.8}Cu_{0.2})_3Ga/SiO_2$. A reverse volcano-type trend was clearly observed in the selectivity change for the SiO_2-supported catalyst, which can be rationalized by two opposite factors. When temperature increases, the selectivity begins to decrease because the hydrogenation ability is enhanced, whereas it turns to increase because ethylene desorption is also accelerated. A similar trend can also be seen in Figure 3c, $(Ni_{0.67}Cu_{0.33})_3Ga/TiO_2$.

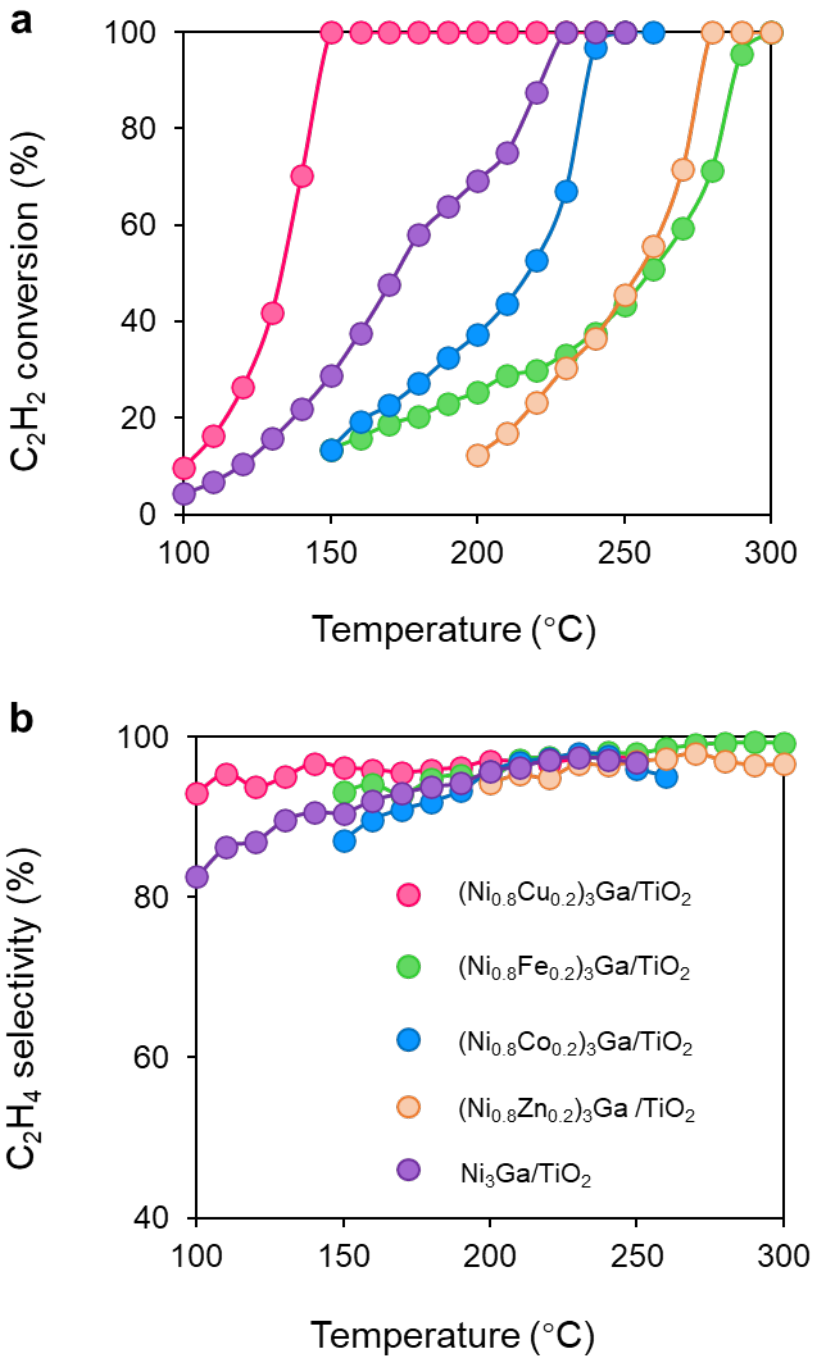

Figure S16. (a) C_2H_2 conversion and (b) C_2H_4 selectivity as a function of reaction temperature over $(Ni_{0.8}M_{0.2})_3Ga/TiO_2$ (M = Cu, Fe, Co, Zn) and Ni_3Ga/TiO_2.

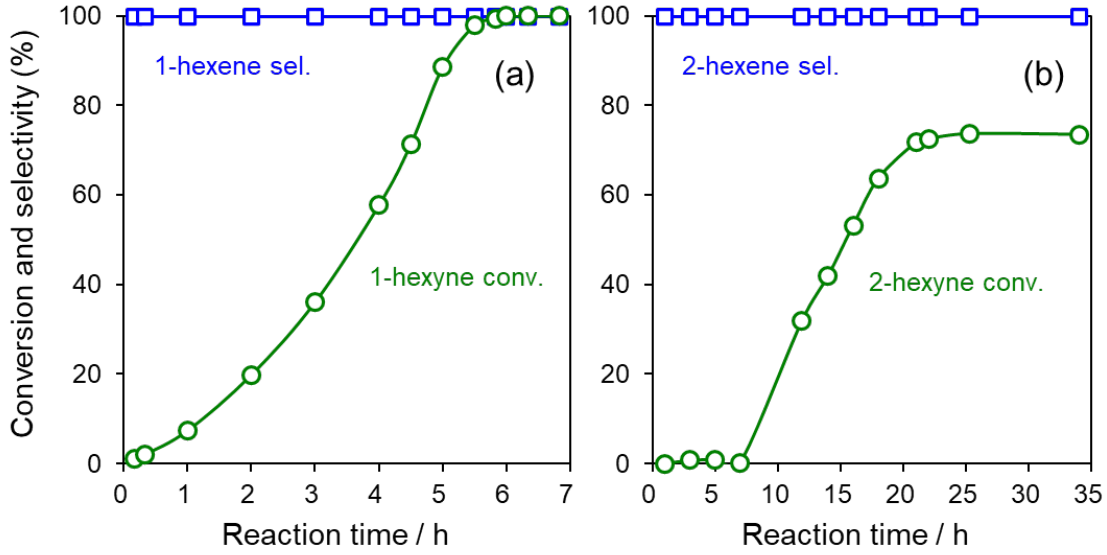

Figure S17. Catalytic performance of $(Ni_{0.8}Cu_{0.2})_3Ga/TiO_2$ in liquid phase hydrogenation of (a) 1-hexyne and (b) 2-hexyne. For 2-hexyne hydrogenation, the reaction occurred after an induction period and did not reach 100% conversion for some reason.

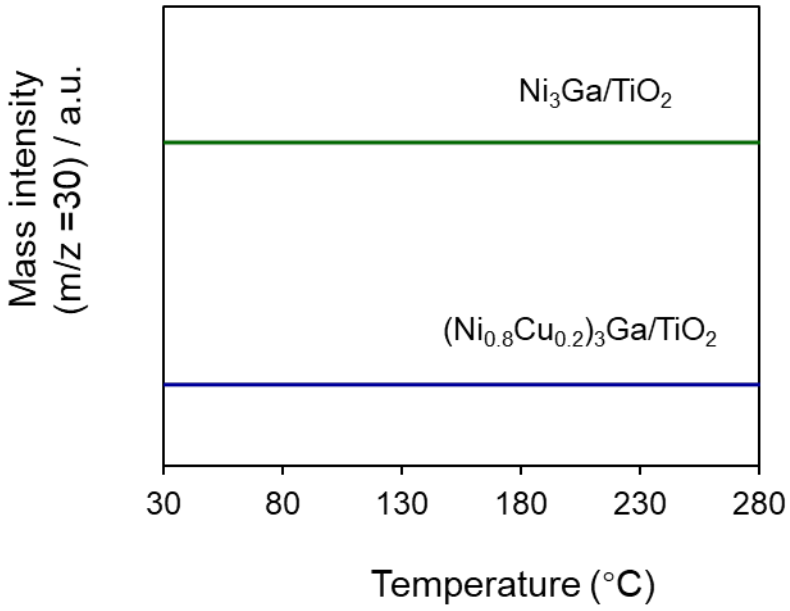

Figure S18. Ethylene temperature programmed surface reaction profiles (TPSR) of the $(Ni_{0.8}Cu_{0.2})_3Ga/TiO_2$ and Ni_3Ga/TiO_2 catalysts for ethylene hydrogenation.

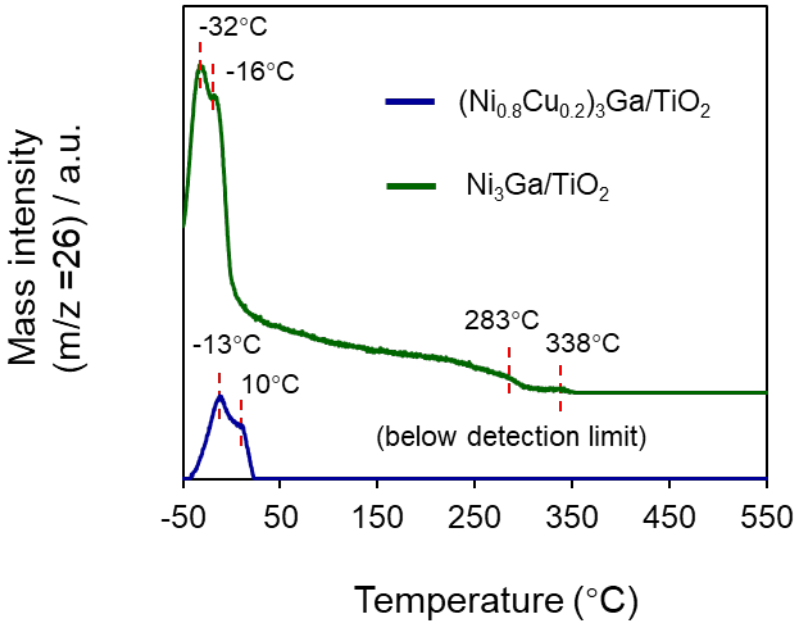

Figure S19. C_2H_2-TPD profiles of the $(Ni_{0.8}Cu_{0.2})_3Ga/TiO_2$ and Ni_3Ga/TiO_2 catalysts.

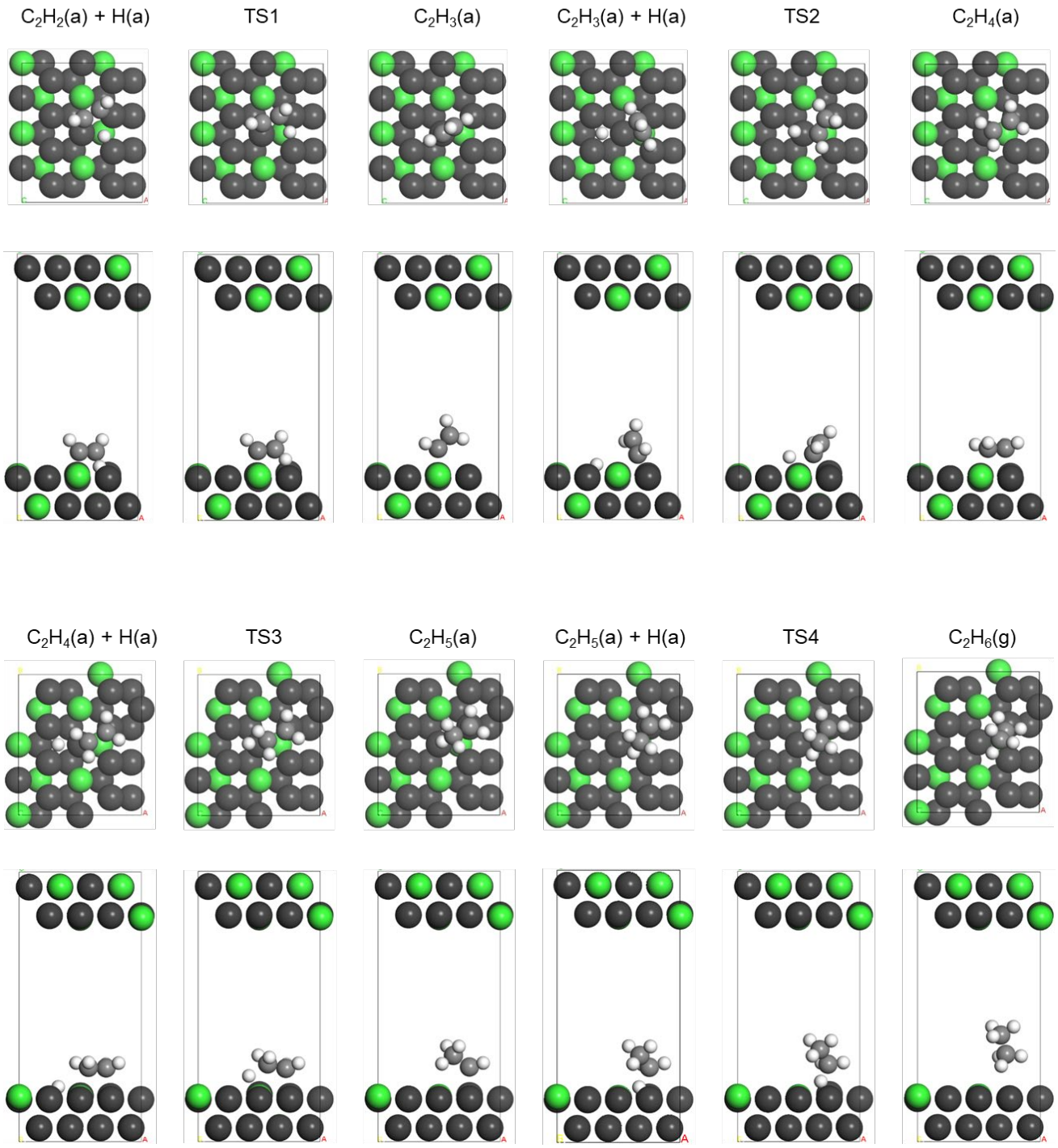

Figure S20. Optimized structures of the slab and adsorbates in acetylene hydrogenation to ethane over $Ni_3Ga(111)$.

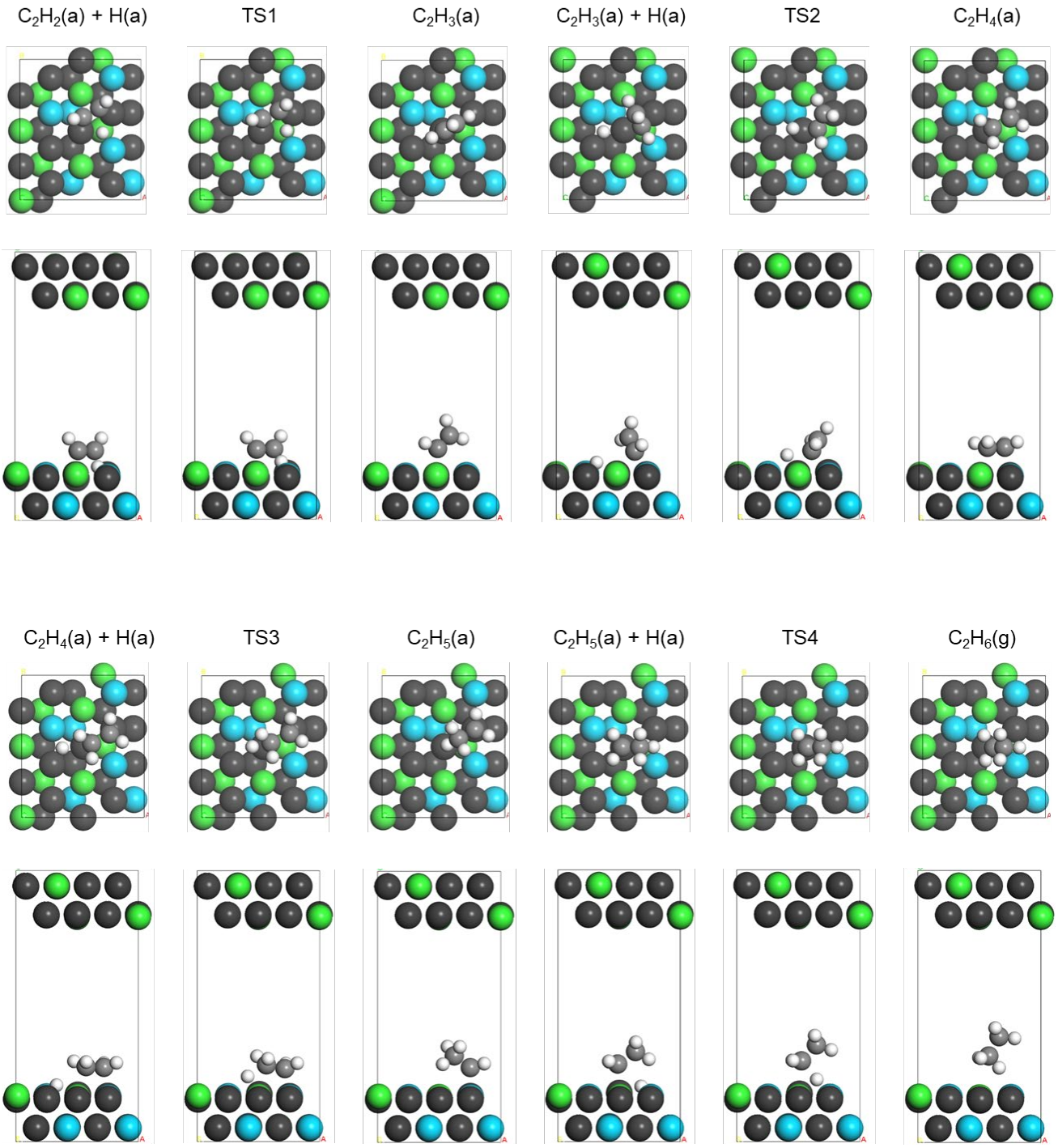

Figure S21. Optimized structures of the slab and adsorbates in acetylene hydrogenation to ethane over $(Ni_{0.8}Cu_{0.2})_3Ga(111)$.

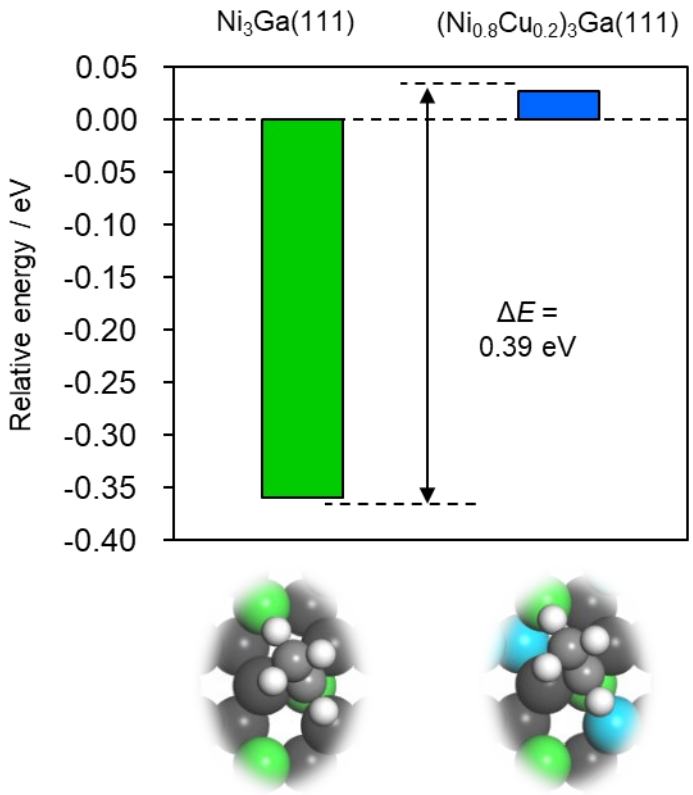

Figure S22. Relative energy of ethylidene intermediate on $Ni_3Ga(111)$ and $(Ni_{0.8}Cu_{0.2})_3Ga(111)$. Sum of gas phase C_2H_6 and the clean slab was set to zero in energy as in Figure 3a.

Supplementary Note

Supplementary References

1 X. Ge, Z. Ren, Y. Cao, X. Liu, J. Zhang, G. Qian, X. Gong, L. Chen, X. Zhou, W. Yuan and X. Duan, *Journal of Materials Chemistry A*, 2022, 19722–19731.

2 B. Fu, A. J. McCue, Y. Liu, S. Weng, Y. Song, Y. He, J. Feng and D. Li, *ACS Catalysis*, 2022, **12**, 607–615.

3 Y. Liu, J. Zhao, J. Feng, Y. He, Y. Du and D. Li, *Journal of Catalysis*, 2018, **359**, 251–260.

4 C. Lu, A. Zeng, Y. Wang and A. Wang, *ACS Omega*, 2021, **6**, 3363–3371.

5 C. Lu, Y. Wang, R. Zhang, B. Wang and A. Wang, *ACS applied materials & interfaces*, 2020, **12**, 46027–46036.
6 Y. Wang, B. Liu, X. Lan and T. Wang, *ACS Catalysis*, 2021, **11**, 10257–10266.
7 H. Liu, M. Chai, G. Pei, X. Liu, L. Li, L. Kang, A. Wang and T. Zhang, *Chinese Journal of Catalysis*, 2020, **41**, 1099–1108.
8 H. Zhou, B. Li, H. Fu, X. Zhao, M. Zhang, X. Wang, Y. Liu, Z. Yang and X. Lou, *ACS Sustainable Chemistry and Engineering*, 2022, **10**, 4849–4861.
9 Y. Cao, H. Zhang, S. Ji, Z. Sui, Z. Jiang, D. Wang, F. Zaera, X. Zhou, X. Duan and Y. Li, *Angewandte Chemie*, 2020, **132**, 11744–11749.
10 X. Shi, Y. Lin, L. Huang, Z. Sun, Y. Yang, X. Zhou, E. Vovk, X. Liu, X. Huang, M. Sun, S. Wei and J. Lu, *ACS Catalysis*, 2020, **10**, 3495–3504.
11 Y. Chai, G. Wu, X. Liu, Y. Ren, W. Dai, C. Wang, Z. Xie, N. Guan and L. Li, *Journal of the American Chemical Society*, 2019, **141**, 9920–9927.
12 J. Gu, M. Jian, L. Huang, Z. Sun, A. Li, Y. Pan, J. Yang, W. Wen, W. Zhou, Y. Lin, H. J. Wang, X. Liu, L. Wang, X. Shi, X. Huang, L. Cao, S. Chen, X. Zheng, H. Pan, J. Zhu, S. Wei, W. X. Li and J. Lu, *Nature Nanotechnology*, 2021, **16**, 1141–1149.
13 F. Huang, Y. Deng, Y. Chen, X. Cai, M. Peng, Z. Jia, J. Xie, D. Xiao, X. Wen, N. Wang, Z. Jiang, H. Liu and D. Ma, *Nature Communications*, 2019, **10**, 4431.
14 C. Riley, A. De La Riva, S. Zhou, Q. Wan, E. Peterson, K. Artyushkova, M. D. Farahani, H. B. Friedrich, L. Burkemper, N. V. Atudorei, S. Lin, H. Guo and A. Datye, *ChemCatChem*, 2019, **11**, 1526–1533.
15 Y. Chen and J. Chen, *Applied Surface Science*, 2016, **387**, 16–27.
16 M. Armbrüster, K. Kovnir, M. Friedrich, D. Teschner, G. Wowsnick, M. Hahne, P. Gille, L. Szentmiklósi, M. Feuerbacher, M. Heggen, F. Girgsdies, D. Rosenthal, R. Schlögl and Y. Grin, *Nature Materials*, 2012, **11**, 690–693.
17 X. Dai, Z. Chen, T. Yao, L. Zheng, Y. Lin, W. Liu, H. Ju, J. Zhu, X. Hong, S. Wei, Y. Wu and Y. Li, *Chemical Communications*, 2017, **53**, 11568–11571.
18 T. Kojima, S. Kameoka, S. Fujii, S. Ueda and A. P. Tsai, *Science Advances*, 2018, **4**, 1–8.
19 J. Ma, F. Xing, Y. Nakaya, K. ichi Shimizu and S. Furukawa, *Angewandte Chemie - International Edition*, 2022, **61**, 1–7.
20 Z. Li, J. Zhang, J. Tian, K. Feng, Z. Jiang and B. Yan, *Chemical Engineering Journal*, 2022, **450**, 138244.
21 Y. Liu, X. Liu, Q. Feng, D. He, L. Zhang, C. Lian, R. Shen, G. Zhao, Y. Ji, D. Wang, G. Zhou and Y. Li, *Advanced Materials*, 2016, **28**, 4747–4754.
22 J. Zhao, L. He, J. Yu, Y. Shi, R. Miao, Q. Guan and P. Ning, *New Journal of Chemistry*, 2021, **45**, 1054–1062.
23 T. Komatsu, T. Kishi and T. Gorai, *Journal of Catalysis*, 2008, **259**, 174–182.
24 B. Bridier and J. Pérez-Ramírez, *Journal of the American Chemical Society*, 2010, **132**, 4321–

4327.
25 F. Fu, Y. Liu, Y. Li, B. Fu, L. Zheng, J. Feng and D. Li, *ACS Catalysis*, 2021, **11**, 11117–11128.
26 X. Ge, M. Dou, Y. Cao, X. Liu, Q. Yuwen, J. Zhang, G. Qian, X. Gong, X. Zhou, L. Chen, W. Yuan and X. Duan, *Nature communications*, 2022, **13**, 5534.
27 S. Zhou, L. Kang, X. Zhou, Z. Xu and M. Zhu, *Nanomaterials*, 2020, **10**, 509.